Nano-colloid based suspensions and emulsions used as means for enhanced oil recovery

Anastasia Strekla[1,2], *Christina* Ntente[1,3], *Maria* Theodoropoulou[1] and *Christos* Tsakiroglou[1,*]

[1]Foundation for Research and Technology Hellas - Institute of Chemical Engineering Sciences, 26504 Patras, Greece
[2]University of Patras, Department of Physics, 26504 Patras, Greece
[3]University of Patras, Department of Chemistry, 26504 Patras, Greece

Abstract. Aqueous solutions of polyphenols extracted from parsley leaves are mixed with solution of ferric chloride hexahydrate to synthesize suspensions of polyphenol-coated iron oxide nanoparticles, which are then used to prepare Pickering oil (n-decane)-in water emulsions. The performance of the nano-colloid suspensions and emulsions as agents of enhanced oil recovery (EOR) is assessed with secondary imbibition tests performed under constant flow rate on a glass-etched pore network, after a drainage / primary imbibition cycle for paraffin oil / brine (0.25M NaCl solution) system. The transient changes of the fluid saturation profile along with the pressure drop across the porous medium are recorded. Comparative analysis of the oil recovery efficiency attained with nano-colloid suspensions of varying iron concentration, and Pickering emulsion, enables us to classify them, and select the most efficient ones for further studies.

1 Introduction

The use of inorganic nanoparticles in petroleum engineering applications including enhanced oil recovery (EOR) has attracted the scientific interest in recent years [1]. An approach to improve the dispersion ability of nanoparticles and tailor their properties for a particular application is to covalently attach polymers to the nanoparticle surface, resulting in polymer-coated nanoparticles (PNPs). While less work has been carried out with PNPs for EOR, recent work suggests they may be superior to unmodified nanoparticles for EOR [2]. PNPs can be tailored for a specific interface and application. PNPs can decrease the interfacial tension of oil and water or water and air, which can lead to more stable emulsions [3-6]. For example, silica nanoparticles coated with a polyelectrolyte were used to stabilize oil-in-water emulsions [7]. More recently, stable oil-in-water emulsions were generated by using silica nanoparticles coated with a pH responsive polymer, and it was found that the most stable emulsions were formed at lower polymer chain grafting densities [8,9]. Related studies on star polymers [10], bottlebrush polymers [11] and paramagnetic particles with adsorbed amphiphilic polymers found stable emulsions [12] and reductions in the oil-water interfacial tension at relatively low (0.1 wt %) particle contents [13]. PNPs can respond to temperature, pH, and light through a change in surface properties [6].

Moreover, significant progress has been done on the development of PNPs for the in-situ remediation of contaminated porous media (e.g. soils, sediments, and aquifers) by injecting zero-valent iron nanoparticles (nZVI) [14-16], and know-how obtained in the context of such environmental studies might be helpful in preparing stable PNPs and designing efficient PNP-based EOR processes [17]. During the last years, green synthesis of NPs has been gaining importance in view of the advantages such as economic benefits, environment friendliness, and recycling. Such 'greener' processes for obtaining various nanomaterials have been widely reported and are gathering attention in several nanotechnology-based applications [18]. As one of the green synthetic approaches, plant extracts were considered for the synthesis of nanoparticles through biosynthetic routes which involve primarily the extraction of polyphenols, which are natural polymers acting as reducing agents and stabilizers [19-21].

In the present work, aqueous solutions of polyphenols extracted from the leaves of parsley are mixed with solution of ferric chloride hexahydrate to produce suspensions of iron oxide nanoparticles, and an ultrasound probe is utilized to generate stable oil-in-water emulsions by mixing the suspensions with n-decane. The performance of the nano-colloid suspensions and emulsions as agents of enhanced oil recovery (EOR) is assessed with secondary imbibition tests performed after a drainage / imbibition cycle for paraffin oil / brine (NaCl solution) system. Displacement tests are conducted under constant flow rate in a transparent glass-etched pore network. The transient changes of the fluid saturation profile along with the pressure drop across the porous medium are recorded. The oil saturation is measured with image analysis of successive snap-shots captured by a CCD camera [22]. Comparative analysis of the oil displacement efficiency attained with nano-colloid suspensions and Pickering emulsions enables us to classify them and pre-select the most efficient ones for further studies.

* Corresponding author: ctsakir@iceht.forth.gr

2 Materials and Methods

2.1 Synthesis of nanoparticles suspensions and emulsions

Initially, 1000 mL of tri-distilled (3D) water were heated to 80 ° C on a hot plate. Then, 50 g of chopped parsley were added in the water and left for 1 hr under stirring at constant temperature. Afterwards, the liquid extract was separated from the solid residue by vacuum filtration with the use of filters of pore size 4 μm, and 2.5 μm (Whatman) and centrifugation at 12000 rpm for 20 min (Heraeus Megafuge-16). The total polyphenol concentration (TPC) of extract was measured in terms of Gallic Acid Equivalent (g/L GAE), by using the Folin-Ciocalteu method [23] and UV-Vis spectroscopy (HITACHI U-3000).

The preparation of the iron oxide nanoparticles (IONP) was accomplished by adding, under stirring, the polyphenol extract (PPH) to a 0.1M $FeCl_3$ solution at a volume ratio 2:1 [24]. The reaction progress was monitored by recording continuously the pH and Redox Potential (ORP), Eh, of the solution with two probes (Vernier pH and ORP electrodes) connected with a data acquisition card (LabQuest Steam) (Fig.1a,b). When pH and Eh were stabilized, the solution colour changed to dark brown signifying the completion of the reaction. After having adjusted its pH to 6.0, the suspension was placed in a refrigerator and kept there until being used.

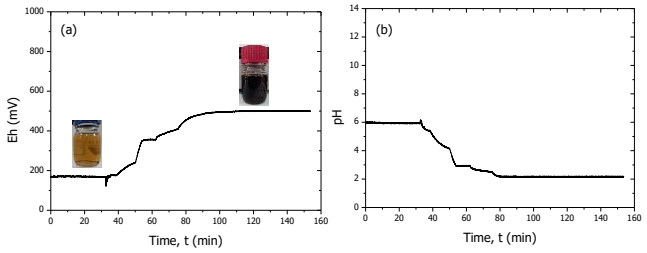

Fig.1. Transient response of the (a) Oxidation Reduction Potential, Eh, and (b) pH of solution, during the synthesis of iron oxide nanoparticles.

The preparation of emulsions was done by mixing 20 mL of aqueous phase (IONP suspension) with 20 mL of n-decane at a volume ratio 1:1 for 10 minutes inside an ultrasonic probe (Hielscher, UP400St).

2.2 Characterization of suspensions

Suspensions of PPH-coated IONPs were prepared at three iron (Fe) concentrations, 0.25, 0.5 and 0.75 g/L. The particle size distribution, and ζ-potential of all IONP suspensions were determined with Dynamic Light Scattering -DLS (Zetasizer Nano System, Malvern) after having diluted each suspension at ratio 1:50 with 3D water.

The surface tension of each solution/suspension, as well its interfacial tension with paraffin oil were measured at 25ºC on a Sigma 702 (KSV Instruments) tensiometer by using the DuNouy Ring method.

The air/water and oil/water static contact angles were measured from images of drops of aqueous phase surrounded by air or oil on a glass plate, using a HY-2307 CMOS camera (Hayear) connected via USB with PC and equipped with image capturing software. The images were analyzed by the OpenDrop software [25].

2.3. Visualization tests

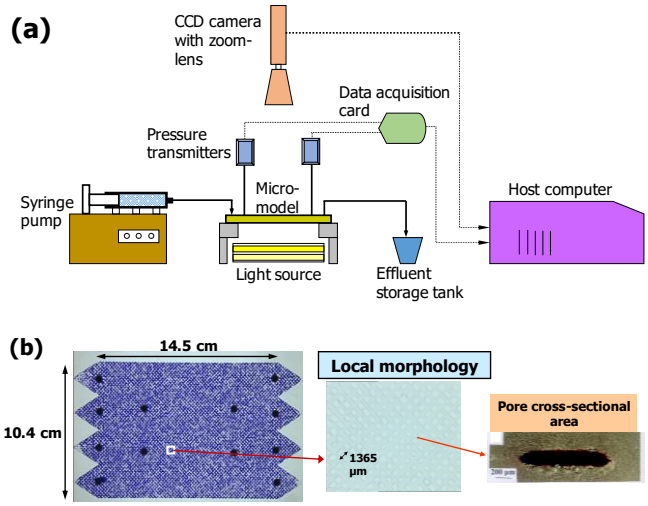

Fig. 2. (a) Schematic diagram of experimental setup. (b) Morphology of glass-etched pore network model.

Immiscible displacement tests were conducted on a glass-etched pore network model (Fig.2a,b). The visualization tests (Fig.2a) enable us to assess the capacity of the various types of NPs to reduce the residual oil remaining in the porous medium after primary drainage (flow rate, q_o=0.08 mL/min) primary imbibition (flow rate, q_w=0.2 mL/min), and secondary imbibition (flow rate, q_w=0.2 mL/min) cycles, where each displacement step started at the point that the previous step stopped, so that a continuous saturation history was recorded. Paraffin oil (Labkem, Spain) colored with oil red (concentration=1500 ppm) was selected as the model viscous oil phase. Aqueous solution of NaCl 0.25M was used as the brine in drainage and primary imbibition tests, and suspension of PPH-coated IONPs, along with its Pickering emulsion with n-decane were used as the displacing fluid in secondary imbibition tests. At each series of displacement tests, images were captured every 10-20 s by a CCD video camera (Panasonic AW-E300E). The pressures were measured continuously on two holes placed on the boundaries of visualized area (Fig.2a) through two pressure transmitters SGM (Electrosystems) properly connected with a data acquisition system (ADAMS-4561 & ADAMS-4117, Advantech). Recorded snap-shots of the flow pattern were processed with image analysis software (ImageJ) to determine the gradual variation of residual oil saturation. (Fig.2a,b).

The capillary number, Ca, and viscosity ratio, κ, are defined by

$$Ca = \frac{u_0 \mu_{inj}}{\gamma_{ow}} \quad (1)$$

$$\kappa = \frac{\mu_{inj}}{\mu_{disp}} \quad (2)$$

where u_0 is the superficial flow velocity (=q/A), μ_{inj} and μ_{disp} are the viscosities of injected and displaced fluid, and γ_{ow} is the oil/water interfacial tension. Moreover, the pore-scale, Ca_{L1} and network-scale, Ca_{LN}, capillary numbers [26] are defined by

$$Ca_{L1} = fCa \quad (2)$$
$$Ca_{LN} = Ca_{L1}(L_N/L_P) \quad (3)$$
$$f = \frac{L_P r_H}{k} \quad (4)$$

where L_N is the network length (L_N=0.14 m), L_P is the pore length (L_P=1.365 mm), r_H is the equivalent hydraulic pore radius (r_H=60 μm) and k the absolute permeability of the porous medium (k=20.5 Da).

3 Results and discussion

The polyphenol concentration in parsley extract, measured by the Folin-Ciocalteu method, was found equal to 2.26 g/L GAE. The physicochemical and interfacial properties of all fluid systems are shown in Tables 1 and 2, respectively.

Table 1. Physicochemical properties of fluid systems

Solution / Suspension	Particle size distribution		ζ-potential (mV)	Density, ρ (g/cm³)
	<D_p> (nm)	σ_p (nm)		
PPH-coated IONPs C_{Fe}=0.25g/L	22.8	6.2	-22.1	0.993
PPH-coated IONPs C_{Fe}=0.25g/L with 0.25 M NaCl	40.2	12.2	-	0.981
PPH-coated IONPs C_{Fe}=0.5 g/	55.0	21.7	-24.7	0.993
PPH-coated IONPs C_{Fe}=0.75 g/L	19.6	7.3	-10.3	0.990

Table 2. Interfacial properties of fluid systems

Solution / Suspension	Surface tension γ_s (mN/m)	Interfacial tension γ_{ow} (mN/m)	Air/water contact angle θ_a (°)	Oil/water contact angle θ_{ow} (°)
PPH solution	55.1	19.4	-	-
0.25M NaCl solution	72.5±0.5	44.0	53.8±0.4	54.5±1.3
PPH-coated IONPs C_{Fe}=0.25g/L	62.8±0.5	27.9	53.1±0.2	39.2±5.9
PPH-coated IONPs with 0.25 M NaCl	57.4±0.25	20.7	55±0.1	43.9±0.4
PPH-coated IONPs C_{Fe}=0.5 g/	57.5±0.3	26.1	51.2±1.2	44.8±0.7
PPH-coated IONPs C_{Fe}=0.75 g/L	53.7±:0.1	20.7	35.2±2.7	11.5±3.2

It is evident that the interfacial properties along with the contact angle are decreasing functions of the iron concentration (Table 1), and the oil displacement efficiency is expected to be favoured when using IONP suspensions of progressively higher Fe concentration. On the other hand, the dynamic surface tension, measured by the pendant drop method is a decreasing function of time (Fig. 3a) revealing the capacity of the system to generate stable foams.

The relative volumes of the various phases as functions of time for a Pickering emulsion synthesized from IONP suspension with C_{Fe}=0.25 g/L and C_{NaCl}=0.25M is shown in Fig.3b.

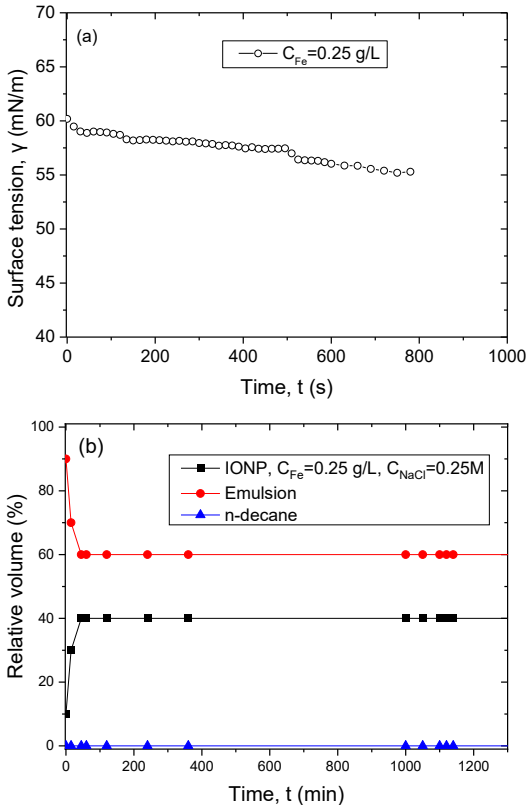

Fig.3. (a) Dynamic surface tension. (b) Transient response of the relative volume of the various phases of emulsion.

Table 3. Experimental conditions

Injected fluid	A	B	C	D
q (mL/min)	0.08	0.2	0.2	0.2
u_0 x 10^5 (m/s)	0.94	2.35	2.35	2.35
μ (Pa s)	0.026	0.001	0.001	0.001
Ca x 10^6	8.0	0.77	0.84	1.13
κ	26.0	0.038	0.038	0.038
Ca_{L1}	0.032	0.0031	0.0034	0.0046
Ca_{LN}	3.32	0.32	0.34	0.47

Injected fluid	E	F	G
q (mL/min)	0.2	0.2	0.2
u_0 x 10^5 (m/s)	2.35	2.35	2.35
μ (Pa s)	0.0125	0.001	0.001
Ca x 10^6	14.1	0.9	1.13
κ	0.48	0.038	0.038
Ca_{L1}	0.057	0.0036	0.0046
Ca_{LN}	5.86	0.38	0.46

*__A__=Paraffin oil; __B__=Aqueous solution C_{NaCl}=0.25M; __C__=IONP solution C_{Fe}=0.25 g/L; __D__=IONP solution C_{Fe}=0.25 g/L C_{NaCl}=0.25 M; __E__=Pickering emulsion; __F__=IONP solution C_{Fe}=0.5 g/L; __G__=IONP solution C_{Fe}=0.7 g/L.

Successive images of the drainage/ primary imbibition/ secondary imbibition steps are shown in Figs. 4-8. Drainage follows a frontal flow pattern (Fig.4a,5a,6a,7a,8a) due to the high viscosity ratio and high Ca_{LN} (Table 3, [26]). The primary imbibition flow pattern is dominated by capillary fingering (Fig.4b, 5b, 6b, 7b, 8b) due to the relatively low value of capillary number at pore, Ca_{L1}, and network, Ca_{LN}, scale (Table 3). Secondary imbibition by IONP suspensions is still dominated by capillary fingering (Fig.4c,5c,6c,7c. Table 3). However, the secondary imbibition by the emulsion transits to a frontal drive (Fig.8c) which is consistent with the increase of the viscosity ratio along with the pore & network scale capillary number by one order of magnitude (Table 3).

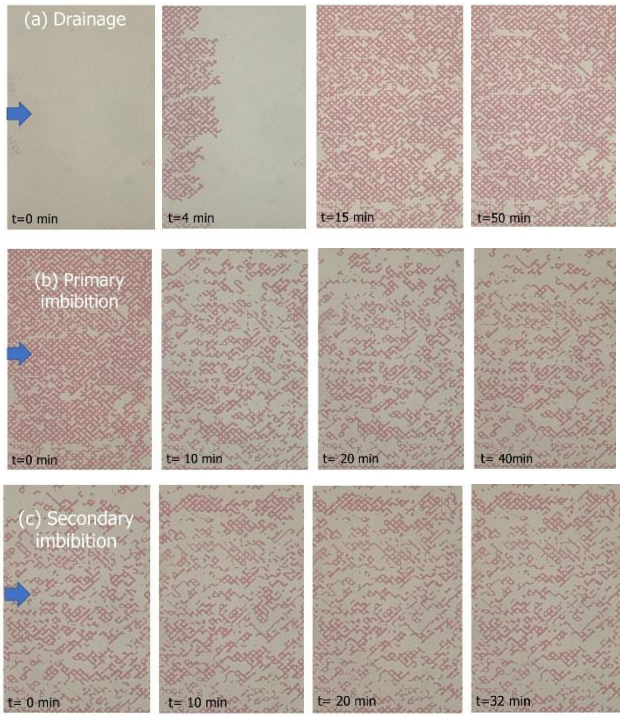

Fig.4. (a) Displacement of brine (C_{NaCl}=0.25M) by paraffin oil (μ=0.026 Pa s). (b) Displacement of paraffin oil by brine (C_{NaCl}=0.25M). (c) Displacement of residual paraffin oil by IONP suspension (C_{Fe}=0.25 g/L, C_{NaCl}=0.25M).

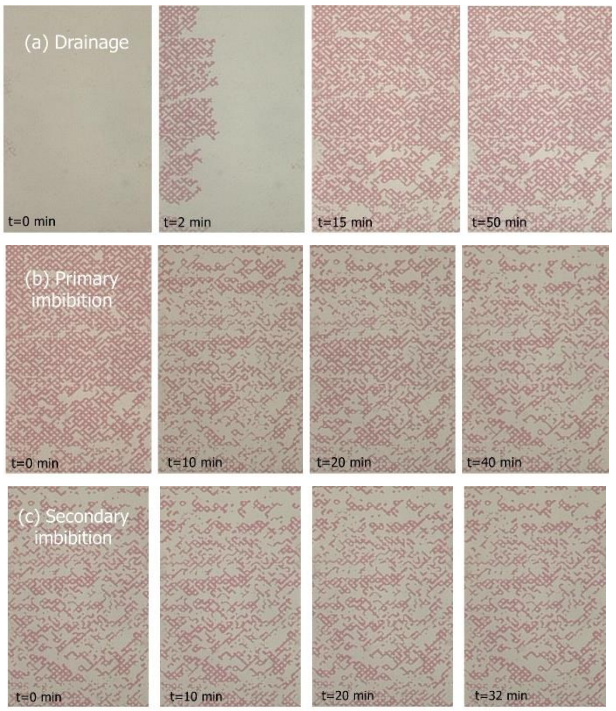

Fig.5. (a) Displacement of brine (C_{NaCl}=0.25M) by paraffin oil (μ=0.026 Pa s). (b) Displacement of paraffin oil by brine (C_{NaCl}=0.25M). (c) Displacement of residual paraffin oil by IONP suspension (C_{Fe}=0.25 g/L).

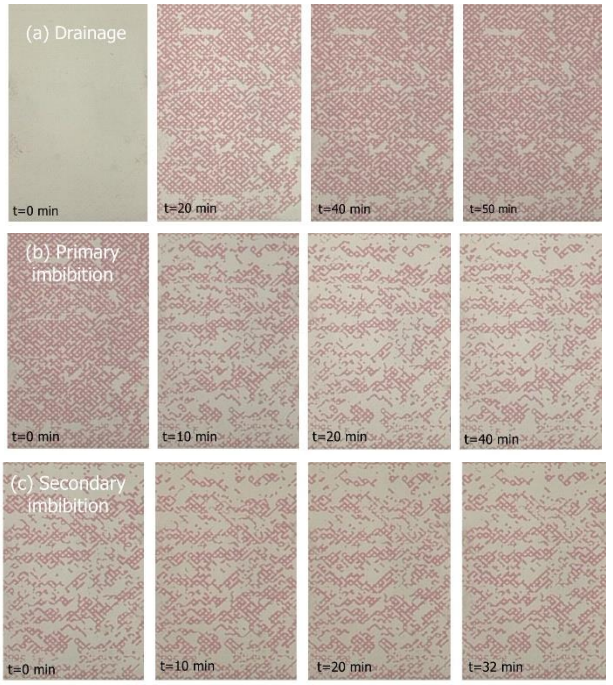

Fig.6. (a) Displacement of brine (C_{NaCl}=0.25M) by paraffin oil (μ=0.026 Pa s). (b) Displacement of paraffin oil by brine (C_{NaCl}=0.25M). (c) Displacement of residual paraffin oil by IONP suspension (C_{Fe}=0.50 g/L).

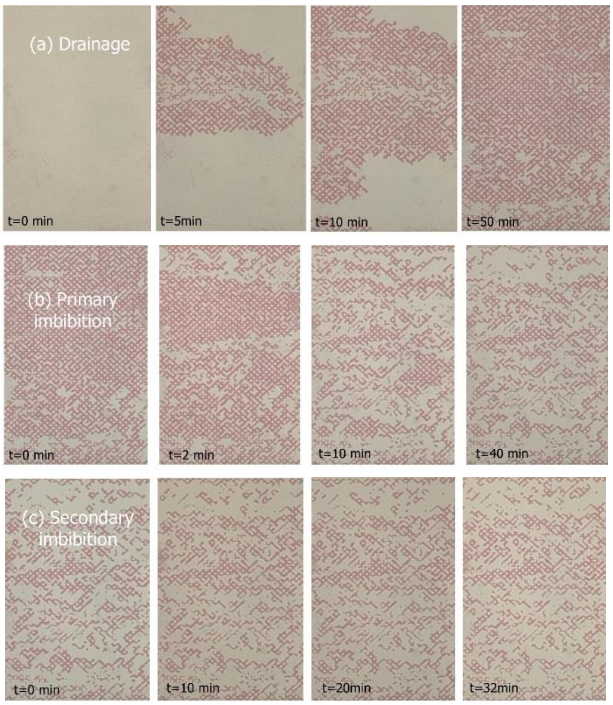

Fig.7. (a) Displacement of brine (C_{NaCl}=0.25M) by paraffin oil (μ=0.026 Pa s). (b) Displacement of paraffin oil by brine (C_{NaCl}=0.25M). (c) Displacement of residual paraffin oil by IONP suspension (C_{Fe}=0.75 g/L).

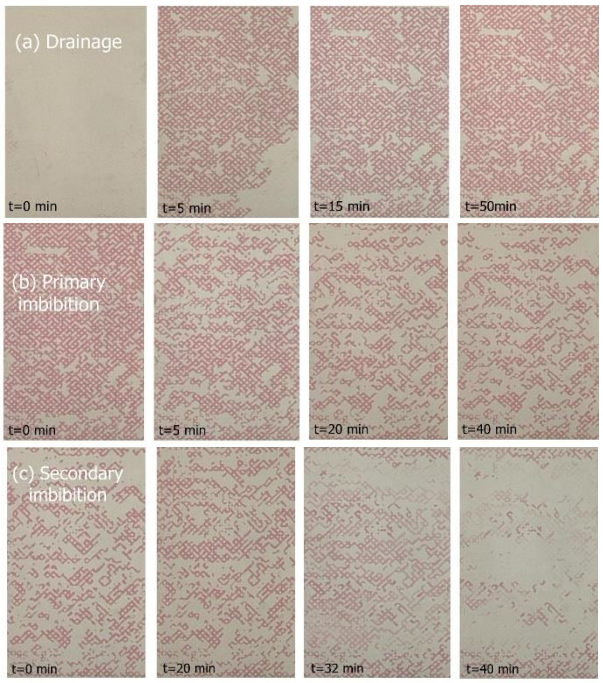

Fig.8. (a) Displacement of brine (C_{NaCl}=0.25M) by paraffin oil (μ=0.026 Pa s). (b) Displacement of paraffin oil by brine (C_{NaCl}=0.25M). (c) Displacement of residual paraffin oil by Pickering emulsion.

During the injection of PPH-coated IONP suspensions, oil trapped at the left side of the visualized area (near the inlet ports) was mobilized and transferred towards the central area, leading to a temporary or permanent increase of oil saturation (Fig.9a-blue circles, Fig. 9b-blue circles, Fig. 9c-green circles, Fig.9d-blue circles). However, on average, the local oil saturation decreases over the majority of pore clusters, at the final stages of the process (Fig.9a,b,c,d). It is worth mentioning that during primary or secondary imbibition, oil mobilization is carried out via a mechanism of successive and locally occurring drainage / imbibition events. On the other hand, the displacement of residual oil by the emulsion follows a clearly frontal-like pattern and is a very efficient displacement, in terms of the percentage of residual oil recovery (Fig.8c).

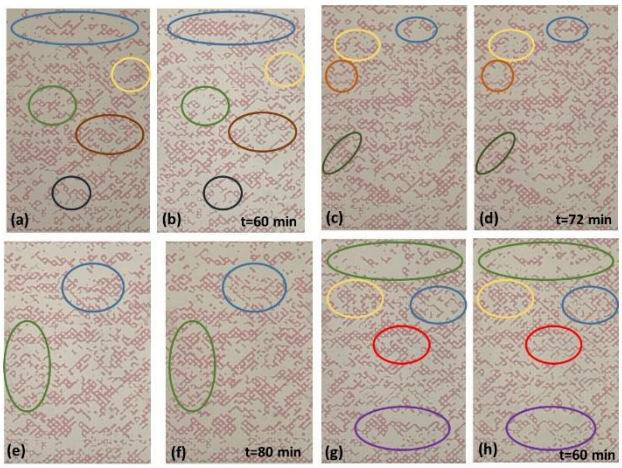

Fig. 9. Comparison between the final snap-shots of primary and secondary imbibition during the displacement of residual oil by (a,b) IONP suspension in brine with C_{Fe}=0.25 g/L, C_{NaCl}=0.25M), (c,d) IONP suspension with C_{Fe}=0.25 g/L, (e,f) IONP suspension with C_{Fe}=0.50 g/L, (g,h) IONP suspension with C_{Fe}=0.75 g/L.

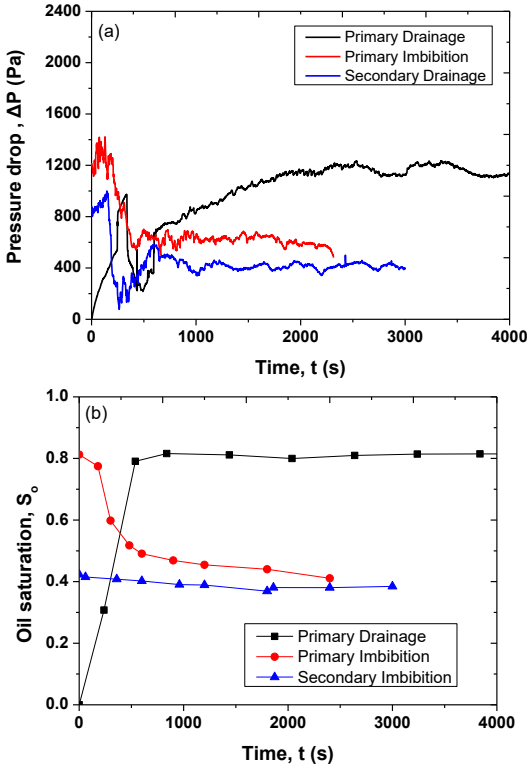

Fig.10. (a) Pressure drop, and (b) oil saturation, as a function of time. IONP suspension with C_{Fe}=0.25 g/L and C_{NaCl}=0.25M was injected at the secondary imbibition step.

The transient response of the pressure drop across the central region of the glass micromodel along with the gradual change of oil saturation are shown in Figs.10-14.

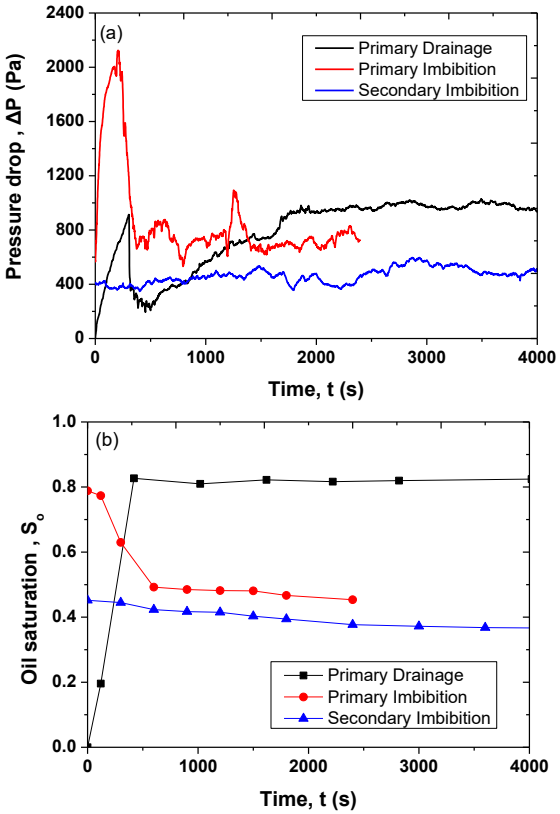

Fig.11. (a) Pressure drop, and (b) oil saturation, as a function of time. IONP suspension with C_{Fe}=0.25 g/L was injected at the secondary imbibition step.

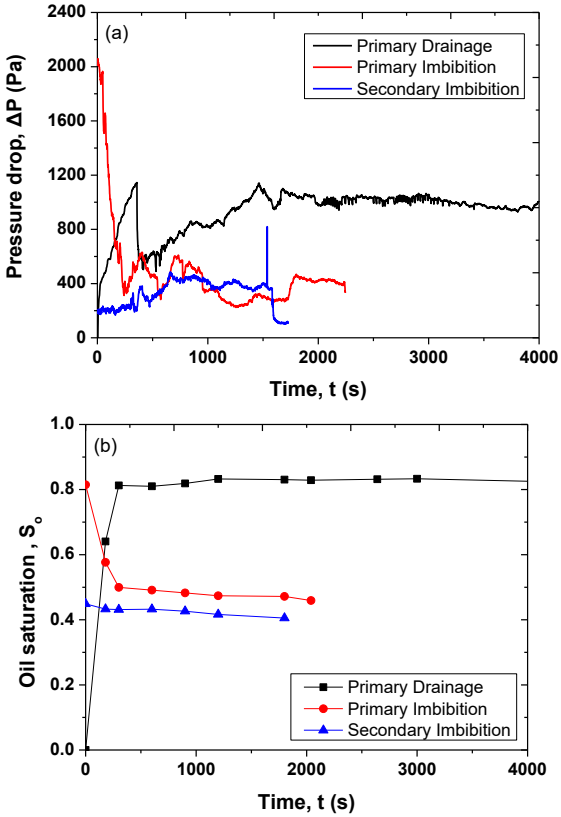

Fig.12. (a) Pressure drop, and (b) oil saturation, as a function of time. IONP suspension with C_{Fe}=0.5 g/L was injected at the secondary imbibition step.

The decrease of the residual oil saturation during the secondary imbibition step by IONP suspensions (Fig.10b,11b,12b,13b) is reflected in the relatively low pressure drop across the porous medium compared to the corresponding one of primary imbibition step (Fig.10a,11a,12a,13a). It is worth mentioning that during secondary imbibition with IONP suspensions, the residual oil displacement efficiency seems to be higher without the presence of NaCl (Fig.11b, 12b, 13b, Table 4). In general, various mechanisms have been proposed in the literature to explain the higher oil recovery with low-salinity water-flooding [27]. Perhaps, oil recovery increases because of changes in the wettability of the porous medium toward more water-wet conditions [27]. On the other hand, it has been observed that at long term, the presence of NaCl favours the destabilization of IONP, their agglomeration, and subsequent precipitation. The high oil recovery efficiency of the secondary imbibition by the shear-thinning Pickering emulsion (Fig.14b) is associated with a relatively high pressure drop across the porous medium, also characterized by strong fluctuations (Fig.14a). The fluctuations are due to the broad range of the viscosity for a shear-thinning fluid (Fig.15): (i) across a single pore [28], as the shear stress varies from zero (at the pore centre) to a maximum (at the pore walls); (ii) throughout the pore network [29,30] between the high and low flow rate regions.

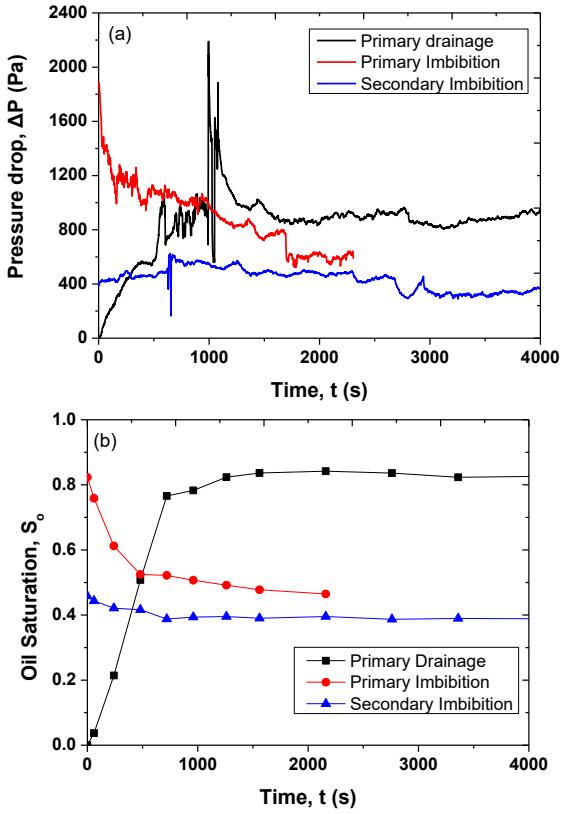

Fig.13. (a) Pressure drop, and (b) oil saturation, as a function of time. IONP suspension with C_{Fe}=0.75 g/L was injected at the secondary imbibition step.

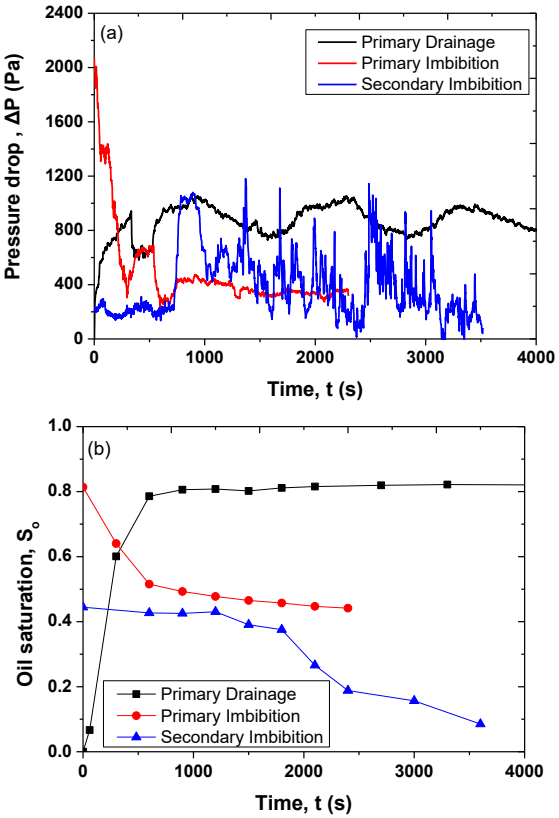

Fig.14. (a) Pressure drop, and (b) oil saturation, as a function of time. Pickering emulsion synthesized from IONP suspension with C_{Fe}=0.25 g/L and C_{NaCl}=0.25M was injected at the secondary imbibition step.

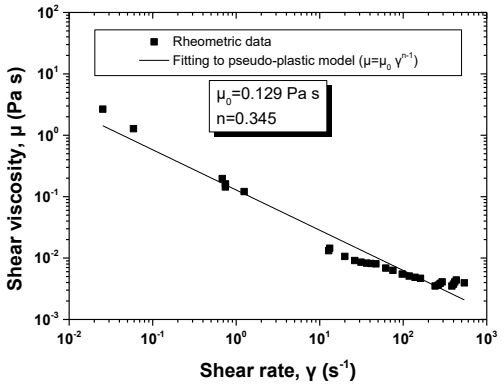

Fig.15. Shear viscosity of emulsion.

Table 4. Summary of results from EOR tests

Displacing fluid in secondary imbibition step	Drainage, S_o	Primary Imbibition, S_o	Secondary Imbibition, S_o	Oil recovery efficiency (%)
IONP C_{Fe}=0.25 g/L	0.815	0.453	0.36	20.5
IONP C_{Fe}=0.25 g/L,C_{NaCl}=0.25M	0.815	0.410	0.386	6.1
Pickering emulsion C_{Fe}=0.25g/L, C_{NaCl}=0.25M)	0.820	0.441	0.085	80.7
IONP C_{Fe}=0.5 g/L	0.818	0.459	0.405	11.7
IONP C_{Fe}=0.75 g/L	0.830	0.465	0.38692	16.7

4 Conclusions

The potential to increase the residual oil efficiency by injecting suspensions of iron oxide nanoparticles synthesized and stabilized by the polyphenols of plant extracts (parsley) is investigated with visualization tests on a glass-etched pore network. Over the investigated experimental conditions, imbibition with IONP suspensions is dominated by the capillary fingering flow pattern. The nanoparticles mobilize trapped oil by transferring it from upstream to downstream through a mechanism of successive steps of drainage (local increase of oil saturation) / imbibition (local decrease of oil saturation). It seems that the oil recovery efficiency of secondary imbibition tests is favored when using IONP suspensions without the presence of NaCl (Table 4). On the other hand, the oil recovery efficiency increases respectably when using Pickering emulsions stabilized by IONP.

Acknowledgements: The research project was supported by the Hellenic Foundation for Research and Innovation (H.F.R.I.) under the "1st Call for H.F.R.I. Research Projects to support Faculty members and Researchers and the procurement of high-cost research equipment" (Project Number: HFRI-FM17-361, acronym: EOR-PNP).

References

1. M.S. Kamal, A.A. Adewunmi, A.A. Sultan, M.F. Al-Hamad, U. Mehmood. J. Nanomat. **2473175**, 1-16 (2017)
2. H. ShamsiJazeyi, C.A. Miller, M.S. Wong, J.M. Tour, R. Verduzco. Appl. Polymer Sci. **131**, 40576, pp.1-13 (2014)
3. T. Sharma, G.S. Kumar, J.S. Sangwai **129**, 221-232 (2015)
4. T. Sharma, S.K. Govindarajan, J. Sangwai. Ind. Eng. Chem. Res. 54, 1576-1584 (2015)
5. N. Bizmark, M.A. Ioannidis, Langmuir **31**, 9282-9289 (2015)
6. N. Kumar, T. Gaur, A. Mandal. J. Ind. Eng. Chem. **54**, 304-315 (2017).
7. N. Saleh, T. Sarbu, K. Sirk, G.V. Lowry, K. Matyjaszewski, R.D. Tilton. Langmuir **21**, 9873-9878 (2005)
8. T. Saigal, H. Dong, K. Matyjaszewski, R.D. Tilton. Langmuir **26 (19)**, 15200-15209 (2010)
9. N. Bizmark, M.A. Ioannidis, Langmuir **33**, 10568-10576 (2017)
10. T. Saigal, A. Yoshikawa, D. Kloss, M. Kato, P. L. Golas, K. Matyjaszewski, R.D. Tilton, J. Coll. Interface Sci. **394**, 284-292 (2013)
11. X. Li, H. ShamsiJazeyi, S.L. Pesek, A. Agrawal, B. Hammouda, R. Verduzco. Soft Matter **10**, 2008-2015 (2014)
12. K.Y. Yoon, Z. Li, B.M. Neilson, W. Lee, C. Huh, S.L. Bryant, C.W. Bielawski, K.P. Johnston. Macromolecules **45**, 5157-5166 (2012)
13. N.J. Alvarez, S.L. Anna, T. Saigal, R.D. Tilton, L.M. Walker. Langmuir **28**, 8052-8063 (2012)

14. C. Tsakiroglou, K. Terzi, A. Sikinioti-Lock, K. Hajdu, C. Aggelopoulos. Sci. Total Env. **563–564**, 866–878 (2016)
15. K. Terzi, A. Sikinioti-Lock, A. Gkelios, D. Tzavara, A. Skouras, C. Aggelopoulos, P. Klepetsanis, S. Antimisiaris, C.D. Tsakiroglou. Coll. & Surf. A: Physicochem. & Eng. Aspects **506**, 711-722 (2016)
16. C.D. Tsakiroglou, A. Sikinioti-Lock, K. Terzi, M.A. Theodoropoulou, *Chem. Eng. Sci.* **192**, 391-413 (2018).
17. D. Arab, A. Kantzas, S.L. Bryant J. Pet. Sci. Eng. **163** 217–242 (2018)
18. A. Sebastian, A. Nangia M.N.V. Prasad. J. Clean. Prod. 174, 355-366 (2018)
19. J. Lin, X. Weng, R. Dharmarajan, Z. Chen. Chemosphere **169,** 413-417 (2017)
20. J. Fowsiya. G. Madhumitha. N.A. Al-Dhabi, M.V. Arasu, J. Photochem. & Photobiol. B: Biology **162**, 395–401 (2016)
21. M. Karavasilis, C.D. Tsakiroglou, Emerging Science Journal **3(6)**, 344-360 (2019)
22. M.A. Theodoropoulou, V. Sygouni, V. Karoutsos, C.D. Tsakiroglou, Int. J. Multiphase Flow **31,** 1155-1180 (2005)
23. M. Geremu, Y. B. Tola and A. Sualeh, Chem. Biol. Technol. Agric. **3:25**, pp.1-6 (2016)
24. V. Kamath, P. Chandra, G.P. Jeppu, Int. J. Phytorem. **22**, 1278-1294 (2020).
25. J.D. Berry, M.J. Neeson, R.R. Dagastine, D.Y.C. Chan, R.F. Tabor, J. Coll. Inter. Sci. **454** 226–237 (2015); http://opencolloids.com
26. C.D. Tsakiroglou, M. Theodoropoulou, V. Karoutsos, , AIChE J., **49,** 2472-2486 (2003).
27. A. Katende, F. Sagala, J. Molec. Liq. **278**, 627-649 (2019)
28. C.D. Tsakiroglou, J. Non-Newt. Fluid Mech. **105**, 79-110 (2002)
29. C.D. Tsakiroglou, J. Non-Newt. Fluid Mech. **117,** 1-23 (2004).
30. C.D. Tsakiroglou, M. Theodoropoulou, V. Karoutsos, D. Papanicolaou, V. Sygouni, J. Coll. Interface Sci. **267,** 217-232 (2003).